Extratropical influence on ITCZ shifts in slab ocean simulations of global warming

Dargan M. W. Frierson
University of Washington

Yen-Ting Hwang
University of Washington

July 2011

ABSTRACT

Recent studies with climate models have demonstrated the power of extratropical forcing in causing the intertropical convergence zone (ITCZ) to shift northward or southward, and paleoclimate data supports the notion that there have been large shifts in the ITCZ over time. It is shown that similar notions apply to slab ocean simulations of global warming. Nine slab ocean model simulations from different modeling centers show a wide range of ITCZ shifts in response to doubling carbon dioxide concentrations, which are experienced in a rather zonally symmetric way in the tropics. Using an attribution strategy based on fundamental energetic constraints, it is shown that responses of clouds and ice in the extratropics explain much of the range of ITCZ responses. There are also some positive feedbacks within the tropics due to increasing water vapor content and high clouds in the new ITCZ location, which amplify changes driven from the extratropics. This study shows the clear importance of simulating extratropical climate responses with fidelity, since in addition to their local importance, the impacts of these climate responses have a large nonlocal impact on rainfall in the tropics.

1. Introduction

One of the most striking sets of papers in recent years is the work of John Chiang and other authors using paleoclimate data and climate models showing that the extratropics can be remarkably efficient in forcing shifts of the intertropical convergence zone (ITCZ). While tropical-extratropical interactions are typically considered as the tropics driving the extratropics, with ENSO being the typical modern analogy (e.g., Horel and Wallace (1981); Hoskins and Karoly (1981)), these recent studies show the dramatic influence the extratropics can have on what is perhaps the most well-known climate feature of the tropics. Chiang et al.

(2003) showed that high latitude land ice, sea ice, or ocean heat transport changes similar to that experienced in Last Glacial Maximum conditions result in a pronounced southward shift of the ITCZ. Chiang and Bitz (2005) showed in particular that a relatively small increase in Northern Hemisphere (NH) sea ice coverage can result in a large southward shift of the ITCZ, with the shifts occurring in all ocean basins in a rather zonally symmetric way. The response is not sensitive to the longitude at which the ice is prescribed. Yoshimori and Broccoli (2008) showed with single-forcing experiments in a slab ocean model that a variety of forcing agents can cause shifts in the ITCZ, including those with peaks in the extratropics such as sulfate aerosols and black carbon. Such extratropical-tropical connections occur in coupled models as well (Zhang and Delworth (2005); Broccoli et al. (2006); Cheng et al. (2010)) and happen quickly even in the coupled setting, within two years (Chiang et al. 2008). Observational evidence is also mounting to suggest that wide excursions of the ITCZ position have occured in the past (e.g., Lea et al. (2003); Koutavas and Lynch-Stieglitz (2004); Pahnke et al. (2007); Sachs et al. (2009)).

Two papers by Sarah Kang and co-authors (Kang et al. (2008); Kang et al. (2009)) introduced a new theoretical framework for interpreting the changes in ITCZ location as a response to extratropical forcing alone. A key ingredient of these theories, as in the work of Yoshimori and Broccoli (2008) and Yoshimori and Broccoli (2009), is the cross-equatorial energy transport in the atmosphere, as this is strongly anticorrelated with any tropical precipitation shift. The anticorrelation is due to the fact that in the deep tropics, the Hadley cell governs both the atmospheric transport of energy (determined by the upper branch of the cell, since the Hadley cell is a thermally direct circulation) and the transport of moisture (determined by the lower branch of the cell, since moisture is confined to the lower atmosphere). As long as the mean circulation dominates in the deep tropics, as it does in observations of the annual mean and seasonal cycle (Trenberth and Stepaniak 2003), and

the ratio of energy transport to moisture transport remains similar, such an anticorrelation is expected.

Simulations described in the Kang et al. papers can exhibit ITCZ shifts from the equator to as far as 20 degrees off the equator when forcing in the extratropics alone is applied. The essential argument in these studies is that an extratropical cooling results in increased baroclinic eddy energy transport into the cooled region, which acts to spread the cooling into lower latitudes. Eventually some of this cooling makes its way into the subtropics, and there an anomalous Hadley circulation develops to assure that upper tropospheric temperature gradients remain small throughout the tropics. This anomalous Hadley circulation transports energy into the cooled hemisphere, but since moisture is carried in the opposite direction as energy, the ITCZ shifts away from the cooled hemisphere.

The Kang et al. (2008) study also showed that the ITCZ shift can be highly sensitive to parameters which affect the modeled responses of clouds. For the same applied extratropical forcing, local or non-local cloud responses can either amplify or damp the applied forcing with different magnitudes. For instance, if low clouds increase in the hemisphere which experiences cooling, this acts to effectively amplify the applied cooling by increasing the shortwave radiation that is reflected away. Any variation in the climate components that contributes to changes in the atmospheric energy budget, for example, changing cloud properties, melting sea ice, or ocean heat uptake/heat transport changes, can affect energy transports in the atmosphere and thus the ITCZ position. In Kang et al. (2008), with identical extratropical forcing, changing model parameters that affect clouds can change the ITCZ response by a factor of two. This result suggests that ITCZ responses in GCMs may be strongly sensitive to the detailed latitudinal structure of the climate components that contribute to changes in the atmospheric energy budget.

In this paper we attempt to identify the causes of ITCZ shifts within slab ocean simu-

lations of global warming from the World Climate Research Programme (WCRP) coupled model intercomparison project phase 3 (CMIP3) multi-model dataset. While the lack of dynamical ocean responses in these simulations imply that they are not useful for forecasts of the future of the ITCZ, these simulations provide a useful simplified context to study the role of energetic source terms in shifting the ITCZ in state-of-the-art atmospheric models. In Section 2, we calculate changes in tropical precipitation and relate this to changes in cross-equatorial energy transports within the models. In Section 3, we utilize the energy budget to perform an exact attribution of the cross-equatorial energy transports into different vertical flux terms. In Section 4 we perform an alternative attribution strategy using an energy balance model (EBM), which accounts for the local temperature response to energy fluxes in a simple way.

2. Precipitation and Atmospheric Energy Budget Changes

a. Changes in precipitation in response to doubling CO_2

We utilize slab ocean simulations from the WCRP CMIP3 multi-model dataset, the slab ocean control experiment and the $2 \times CO_2$ equilibrium experiment. We calculate climatologies using the last 20 years of data for each model. There are 9 models which have adequate data in both of these experiments for our full analysis: MPI ECHAM5, GFDL CM2.0, MIROC (medres), INM CM3, UKMO Hadgem1, CCCMA CGCM3 (T63), CCCMA CGCM3 (T47), MIROC (hires), and MRI CGCM2.

We first plot zonally averaged precipitation changes with doubled CO_2 in the nine models in Figure 1(a). Familiar features are seen in the precipitation changes: moistening in

the tropics and mid- to high-latitudes, and drying in the subtropics (Held and Soden 2006). In the tropics however, there are large differences among models in the zonally averaged responses. For instance, near 10° N, one model simulates an increase in precipitation of 50 cm/yr, while another model shows a decrease of over 10 cm/yr. Large precipitation disparities are not confined to the NH either. Over 10 cm/yr differences in simulated precipitation change are common between 20° S and the equator.

There are two main reasons for the discrepancies in the projected change of tropical precipitation in these simulations. First, the climatology in the control experiment is different from model to model, with varying degrees of double ITCZ problem (Lin 2007), and the latitude of maximum zonal mean precipitation ranges from the equator to 9N. The projected change of precipitation partly depends on the precipitation in the control experiment, as already wet regions tend to moisten the most (Held and Soden 2006). Models that have the ITCZ further north in the control experiment tend to have more increase in precipitation further north. The second main reason for discrepancies in tropical precipitation, which explains more variance than mean state differences, is north-south shifts in the ITCZ. As shown in Figure 1(a), models that increase their precipitation more on the northern side of the ITCZ also exhibit more of a decrease on the southern side, and vice versa. The shift also extends to the subtropics, where models experiencing a northward ITCZ shift exhibit a larger drying trend in the Southern Hemisphere (SH) subtropics. In this paper, we will focus on understanding the discrepancies related with north-south shifts of tropical precipitation.

To demonstrate how zonally uniform the changes are, we also plot the change in precipitation as a function of latitude and longitude in Figure 2. In most models, the shift occurs across both land and ocean. Drying in the subtropics appears across all longitudes, with MPI, GFDL, and MIROC (medres) experiencing more drying in the SH subtropics, and MRI and CCCMA(T63) experiencing more drying in the NH subtropics.

b. Changes in energy transport

We next calculate the change in atmospheric energy transport which is plotted in Figure 1(b). We assume the atmospheric energy budget is in steady state so the equation for the change in energy budget is

$$\nabla \cdot \mathbf{F_A} = Q_S - Q_L - Q_O \tag{1}$$

where $\mathbf{F_A}$ is the vertically integrated atmospheric moist static energy transport, Q_S is the net shortwave radiation at top-of-atmosphere (TOA), Q_L is the outgoing longwave radiation (OLR), and Q_O is the net downward surface flux. Each variable represents the change between doubled CO_2 and the control climatology. Meridional energy transports are calculated in the GCMs by integrating Equation 1:

$$F_A = \int_{-\frac{\pi}{2}}^{\phi} \int_{0}^{2\pi} (Q_S - Q_L - Q_O) a^2 cos\phi d\lambda d\phi \tag{2}$$

where F_A is the meridional component of the energy flux, a is the radius of the Earth, ϕ is latitude, and λ is longitude. The primary feature of Figure 1(b) is an increase in poleward energy transport of varying magnitude in both hemispheres, shown in Hwang et al. (2011), and explained by increased atmospheric moisture content in Hwang and Frierson (2010). Model-to-model differences are explained in Hwang and Frierson (2010) by differences in the climate components that contribute to changes in the atmospheric energy budget in each model, with cloud effects causing the largest spread.

The change of cross-equatorial atmospheric energy transport varies significantly from model to model, with 4 models having a northward transport at the equator and 5 models with a southward transport. Most of the profiles are essentially linear in the deep tropics, so the cross-equatorial value is typical of any kind of symmetric latitudinal average across the equator (e.g., 5° N to 5° S or 10° N to 10° S).

c. Changes in precipitation and cross-equatorial fluxes

Models are colored in Figure 1(a) in order of their cross-equatorial atmospheric energy transport change from Figure 1(b). It is clear that the models with more southward energy transport at the equator are the models which exhibit a more northward-shifting ITCZ (blue colors), and models that moisten the southern side of the tropics have a northward transport of energy at the equator (red colors). To quantify the ITCZ shift, we calculate the shift of the precipitation center, which is defined as the latitude that is the centroid of the area-integrated precipitation from 15S to 15N. We plot this precipitation shift index versus the cross-equatorial energy transport in Figure 3(a); the correlation coefficient is 0.93. The intercept of the best-fit line is also near zero, meaning models with no ITCZ shift also have near-zero cross-equatorial energy transport change. This result indicates that changes in the mean meridional circulation (the Hadley circulation) are governing the dynamics in the deep tropics. Models which transport energy northward across the equator by the upper branch of the Hadley circulation also transport moisture southward across the equator, resulting in a southward ITCZ shift. While this result is not surprising given the importance of the mean Hadley circulation in shaping the ITCZ in the current climate, it does imply that if one can explain the cross-equatorial energy transport then such a theory explains the zonally averaged precipitation shifts as well.

d. Changes in precipitation and hemispheric temperature changes

Another quantity that one might expect to be correlated with shifts in tropical precipitation is the inter-hemispheric difference in surface warming (e.g., Broccoli et al. (2006) and Yoshimori and Broccoli (2008), although the latter study found the cross-equatorial energy flux to be more highly correlated with the tropical precipitation shifts across a range of

simulations). We correlate the same precipitation shift index described above with the 2 meter air temperature change averaged in the NH minus SH in Figure 3(b). The correlation remains relatively high (0.83), indicating that the models which show more of a northward shift of tropical precipitation are indeed those which warm the NH more. However, all models show more warming in the NH than the SH, while 4 models show a southward shift of tropical precipitation. The y-intercept of the best fit line is thus away from zero, and the temperature change is thus a poorer predictor of the tropical precipitation shift as compared with the energy flux. We return to the role of interhemispheric temperature differences later in the paper.

3. Vertical Energy Fluxes and the Cross-Equatorial Energy Transport

Having shown in Section 2 that tropical precipitation shifts are highly correlated with cross-equatorial energy transports, we next perform attribution studies to explain the cross-equatorial energy transport in each model. In this section we use the atmospheric energy budget to divide the cross-equatorial flux into contributions from vertical energy fluxes at each latitude. This technique is exact and has been used in several other studies (e.g., Wu et al. (2010); Donohoe and Battisti (2011); Zelinka and Hartmann (2011)). The primary disadvantage of this technique, explained in detail in Section 3c, is the fact that in response to a given vertical energy flux, for example, a shortwave heating in the NH due to a reduction in cloud cover, the atmosphere responds both by fluxing energy into the SH and by increasing temperature and OLR locally within the NH. In the technique in this section, these contributions are counted as separate terms, i.e., the shortwave cloud warming causing

a southward cross-equatorial flux, and the OLR increase causing a northward flux. With this difficulty in mind, our technique in Section 4 introduces an EBM which allows calculation of the partition into energy fluxed away versus radiated to space locally due to each term.

a. The effects of vertical energy fluxes on the cross-equatorial energy transport

From Equation 2, the change of poleward energy transport F_A can be decomposed into individual vertical energy flux terms into the atmosphere. We plot the total energy input into the atmosphere $Q_A = Q_S - Q_L - Q_O$ in Figure 4(a), with the x-axis scaled as $sin(\phi)$ since area-integration must be performed in the meridional transport calculation. The change of cross-equatorial energy transport $F_A(\phi = 0)$ can be expressed as either the integral of Q_A from 90° S to the equator, or the equator to 90° N:

$$F_A(\phi = 0) = \int_{-\frac{\pi}{2}}^{0} \int_{0}^{2\pi} Q_A a^2 cos\phi d\lambda d\phi \tag{3}$$

$$= -\int_{0}^{\frac{\pi}{2}} \int_{0}^{2\pi} Q_A a^2 cos\phi d\lambda d\phi, \tag{4}$$

defining the net vertical heat input into the atmosphere $Q_A = Q_S - Q_L - Q_O$. As CO_2 is doubled, models which have more anomalous heating in the NH and cooling in the SH require an increase in southward cross-equatorial transport to be in energy balance. One model, MRI, has a large heating in the deep tropics which requires a large northward transport to balance. But in many models the energetic differences come from higher latitudes. To examine the latitudes which cause the inter-model spread in the change of cross-equatorial energy transport in more detail, we write 3 and 4 as

$$F_A(\phi = 0) = \frac{1}{2}\left(\int_{-\frac{\pi}{2}}^{0} \int_{0}^{2\pi} Q_A a^2 cos\phi d\lambda d\phi - \int_{0}^{\frac{\pi}{2}} \int_{0}^{2\pi} Q_A a^2 cos\phi d\lambda d\phi\right). \tag{5}$$

Motivated by this identity, we plot the integrand $\frac{1}{2}(Q_A(-\phi) - Q_A(\phi))$ in Figure 4(b), to identify which latitude bands are most important in creating a cross-equatorial transport.

When this diagnostic is positive at a particular latitude, this means that the SH receives more energy input than the NH at this latitude, and the atmosphere thus requires a northward cross-equatorial transport to preserve energy balance. In Figure 4(b), one can see that different latitude bands are important in different models in creating a cross-equatorial energy transport. There is uniformly large inter-model variance at all latitudes poleward of 50 degrees, with differences of 5-10 W/m^2 typical for models at these latitudes. It is also notable that models which experience a more southward cross-equatorial transport (blue colors) are identifiable as more negative in Figure 4(b) in the extratropics, while red-colored models have primarily positive values. Latitudes between 30 and 45 experience comparitively smaller variance in Figure 4(b), with most models near zero. Two models have a large difference in the subtropics between 15 and 30 degrees, the MIROC(hires) and MPI ECHAM5 model, which appears to explain some of the change in cross-equatorial energy transport in these models. Only the MRI model has a large positive value in the deep tropics.

b. Latitudinal Distribution of Individual Energy Source Terms

We next examine individual energy source terms and their hemispheric asymmetry to perform a partitioning of the cross-equatorial energy transport change in each model using Equation 5. We separate Q_A in Equation 5 into changes due to individual energy source terms. The energy source terms we discuss in this paper refer to the changes of the atmospheric energy budget due to variations of individual climate components, such as clouds, surface albedo, and water vapor. The global mean of these energy source terms, if divided by global mean temperature change, are often referred to as climate feedbacks in climate sensitivity studies.

The change in net solar radiation Q_S is partitioned into three energy source terms: surface albedo (I), cloud shortwave effects (C_S), and non-cloud scattering and absorption (N_S),

using the approximate partial radiative perturbation (APRP) method (Taylor et al. 2007) to separate these terms accurately. The sum of the three terms is the same as the difference in net incoming shortwave radiation between the $2 \times CO_2$ and the control experiment. OLR changes (Q_L) are partitioned into those due to water vapor (WV), temperature (T) (including both Planck and lapse rate effects), and cloud longwave effects (C_L), using the radiative kernel method (Soden et al. 2008), with kernels constructed from the GFDL model. There is a nonnegligible residual term (R_L) when comparing the sum of all of the LW terms with the difference in net longwave radiation between the $2 \times CO_2$ and the control experiments as we discuss later in this section. Further experiments with each model would be desirable to verify the accuracy of the radiative partitioning methods, but are beyond the scope of this study. The zonal mean of each energy source term is plotted in Figure 5, 6, and 7. Similar with Figure 4, the antisymmetric component of each term is plotted next to its latitudinal distribution. Note that if models are stacked red to blue from top to bottom in the antisymmetric component for a particular term, then that indicates a component that explains some of the model-to-model spread in the changes of cross-equatorial energy transport. The implied cross-equator energy transport change calculated by integrating each energy source term (following Equation 5) after removing its global mean is plotted in Figure 8. Each dot is the result of one model. Positive values imply this particular energy source term requires an increase in northward energy transport at the equator and thus may shift the ITCZ southward. Again in Figure 8 if models are stacked red to blue, it indicates a positive contribution to the model-to-model spread.

The water vapor effect (WV) is greatest in the tropics and generally declines from the equator to the poles (Figure 5(a)). This is due to the fact that there are only small changes in relative humidity in these simulations, which implies a preferential increase in the specific humidity of the tropics. However, the constant relative humidity framework is not sufficient

when one wants to understand the hemispheric asymmetry of the water vapor effect. Figure 5(e) shows that models with more northward shift of ITCZ (blue models) are also the models experiencing more positive water vapor effect in NH tropics. This feature should be considered as a response to the ITCZ shift, with higher moisture content and a larger water vapor greenhouse effect in the hemisphere into which the ITCZ shifts. The heating from the WV greenhouse effect then acts as a positive feedback that drives a larger shift of ITCZ in the same direction. Such a positive feedback to ITCZ shifts from WV has been previously identified in the study of Yoshimori and Broccoli (2009).

There are two other feedbacks that result from shifts in the ITCZ which we discuss next: when the ITCZ shifts from north to south, in addition to humidification of the south, there are also increases in the cloud greenhouse effect and increases in reflected SW radiation in the south (with opposite changes in the north), both resulting from the increased high cloud cover where the ITCZ has shifted. The LW cloud effect (C_L) also acts as a positive feedback for shifts. Figure 5(f) shows the hemispheric asymmetry of the cloud LW effect. Models show increasing high cloud coverage at the new ITCZ location, which results in decreasing OLR and a net heating. This also leads to a cross-equatorial energy transport in the opposite direction and shifts the ITCZ farther. The increasing cloud LW effect extends into the subtropics in many cases.

A negative feedback occurs in the deep tropics for the cloud SW effect (C_S) (Figure 5(g)). For instance, in the models that show a northward shift (blue models), there is more negative cloud SW effect in NH tropics due to increases in cloud fraction. All of the models beside MRI (dark red) show a strong anti-correlation between cloud LW and cloud SW effects in the tropics. Therefore, summing the two (Figure 5(h)) eliminates much of the positive/negative feedback of these terms.

Outside of the tropics, it is clear that clouds are a primary factor influencing the cross-

equatorial transport. The cloud SW effect in particular dominates the hemispheric asymmetry in mid- to high latitudes. In the extratropics, models that experience more cooling from cloud SW effects in the SH compared with NH tend to create a southward cross-equator transport and a northward ITCZ shift (blue models), and vice versa. The largest model-to-model spread comes from differences in the 50-70 degree latitude band, which contributes approximately twice as much variance as other latitude bands, but essentially all latitudes contribute to some cross-equatorial transport. As shown in $C_L + C_S$ in Figure 8, clouds contribute most of the spread in the change of cross-equator transport, even after combing their SW and LW effect.

Changes in SW radiation associated with surface albedo also explain a large amount of the model-to-model spread (Figure 6(a)(e) and I in Figure 8). The hemispheric asymmetry plot (Figure 6(e)) demonstrates the differences in changes in snow and sea ice in the two hemispheres. In midlatitudes, there is more snowpack melted in the NH, which results in a negative value for the SH minus NH asymmetry index. In high latitudes, however, all of slab models predict more sea ice melting near Antarctica than in the Arctic (this is very different from results from coupled GCMs). Models experiencing more heating from melting sea ice in the SH (red models) tend to be the models that simulate northward cross-equator energy transport and southward shift in the ITCZ (I in Figure 8).

Changes in upward surface flux (O) are non-negligible despite the fact that these are equilibrium simulations with slab ocean models (Figure 6(b)(f) and O in Figure 8), where the ocean should not contribute to changes in atmospheric energy budget. Much of the non-zero parts of this term is near the sea ice edge, where Q-fluxes are revealed when sea ice melts (Figure 6(b)), so Q-fluxes are not necessarily constant in the simulations.

The non-cloud SW term (N_S) calculated by the APRP method describes the changes of SW fluxes at the TOA that are not associated with clouds or surface albedo. This includes

absorption changes from increasing water vapor and CO_2 which provide an approximately globally uniform background positive value. The APRP method is less accurate in the high latitudes where the surface albedo changes are particularly large.

The LW residual term (R_L) is the difference between the actual change in LW flux at TOA and the sum of water vapor effect, temperature effect, and cloud LW effect, as shown in Figure 6(d). This term includes the radiative forcing from doubling CO_2, so all models are positive and have global averages from $2.5 - 5W/m^2$. Also included in this term are errors in the kernel method, which are likely non-negligible since only the kernel calculated from the GFDL model control climatology is used (radiative kernels cannot be constructed for each individual model with the limited data stored in the CMIP3 archive). Additionally nonlinear effects are included in this term, since the kernel method assumes the energy source terms are linear. A particularly important feature of the LW residual term is that it is anticorrelated with the LW cloud and WV effects in models, likely due to nonlinear interactions between these two effects. The LW residual thus causes a negative feedback to the cross-equatorial flux, implying that some of the positive feedbacks of these terms are likely slightly overestimated.

c. The Role of Local Temperature/OLR Increases

In this section we have performed an exact partitioning of the change of cross-equatorial transport into different energy source terms, all except for the local temperature effect. We next give a caveat to this method of partitioning, mentioned briefly in the introduction to Section 3, involving compensating local OLR changes due to the temperature response to energy source terms. By performing a direct integration to get the implied cross-equator transport of each term, we implicitly assume that the heating at a particular latitude would be felt uniformly at all latitudes through energy transports. However, in reality, heating at a

particular latitude is also associated with a local warming and humidification, and increases in the OLR associated with the temperature increase. In other words, some of the heating will be balanced by increasing OLR, and will not result in a change in transport.

In Figures 7 (a)-(c), we plot the temperature effect, the sum of temperature and water vapor effects and the sum of all of the other terms, and Figures 7 (d)-(f) are the antisymmetric parts of these terms. We consider the sum of temperature and water vapor effects since warming is typically also associated with humidification. Figure 7(e) shows that the sum of water vapor and temperature effects in the extra-tropics is anti-correlated with the sum of all of the other terms (Figure 7(f)), and with the ITCZ shift in general. Models that have less anomalous heating in the SH extratropics (blue models) tend to show less increase in OLR there (positive value in Figure 7(e)). In the tropics, the positive water vapor feedback discussed in last section dominates. Models with a southward ITCZ shift (red models) tend to show more enhanced greenhouse effect and less OLR increase from WV and temperature in the SH tropics (positive value in Figure 7(e)). In WV+T in Figure 8, it is shown that the anticorrelation in the extratropics dominates over the positive feedback in the tropics, and results in a negative feedback on ITCZ shifts (blue dots over red dots).

In addition, there is a clear tendency for $WV+T$ in Figure 8 to be positive for all models, meaning it causes a northward cross-equatorial energy transport, and a southward shift of the ITCZ. This reflects the fact that non-cloud OLR increases are larger in the NH than the SH for all models. This is presumably due to the fact that the NH is easier to warm and more difficult to humidify than the SH. The energetic partitioning suggests an interesting mechanism for ITCZ shifts, proposed first by Zelinka and Hartmann (2011): despite the tendency of the NH to warm more quickly, the increased OLR resulting from the warming leads to an ITCZ shift away from the warmed hemisphere, when this temperature effect is considered on its own. The general anticorrelation of this component with the total cross-

equatorial transport change shows however that models that tend to warm the NH more do indeed have more of a northward shift of the ITCZ.

The local warming response to energy source terms is sufficient to offset a large amount of the energy input. The partition we performed in the last section may overestimate the importance of individual energy source terms, particularly in high latitudes, because much of a given heating will be balanced by local temperature responses. This implies that for the most accurate attribution, one must additionally take into account the change in longwave flux that would occur if each energy source term was removed. We attempt to perform such an attribution with an EBM in the next section.

4. Prediction and Attribution of ITCZ Shifts with an EBM

To consider the increasing non-cloud OLR as a response to other energy sources, we introduce an EBM to predict the change in meridional energy transport due to each energy source term (Hwang and Frierson (2010)). The EBM responds to a localized heating at a particular latitude with both a local increase in OLR and increased diffusive transport away, with the partition between the two determined by a diffusivity constant. Therefore, it provides a better estimate of how the energy transport changes due to a particular energy source term. A downside to the EBM attribution method, of course, is that it calculates an approximation to the cross-equatorial energy flux rather than using the exact values as in the method of Section 3.

The EBM uses a latitudinally constant diffusivity for moist static energy which is the same value for all models and in both the control and the $2\times CO_2$ experiments, and is tuned to

fit the multi-model mean control climate. Longwave radiation is parameterized as a linear function of temperature using a regression from the control experiment, and 80% surface relative humidity is assumed. The EBM is run with shortwave radiation, total surface flux, and longwave cloud radiative forcing as inputs to generate a mean climatology. The model is then run under warmed conditions, with shortwave radiation changes, longwave cloud radiative forcing changes, and surface flux changes. The model predicts energy transport, temperature, and clear sky longwave radiation in both experiments.

Most of the energy source terms we include in the EBM are the same as the integration method used in the last section. The only two differences are: (1) we use the change in LW cloud radiative forcing instead of the radiative kernel method to estimate the LW cloud radiative effect, to be consistent with the outgoing LW radiation in control experiment used to tune the EBM and (2) we do not prescribe the water vapor and temperature effects, but let the EBM determine the changes in LW associated with these two effects. The predictions of cross-equatorial energy transport predicted by the EBM versus the actual changes in the models are plotted in Figure 9. The EBM does an excellent job of separating the models, with correlation coefficient R = 0.91. Combined with the result from Figure 3 that the ITCZ shift is well-correlated with the cross-equatorial MSE transport, this implies that the EBM can also explain the range of ITCZ shifts in the simulations. The correlation between ITCZ shift and EBM predicted cross-equatorial transport is 0.92.

There is a systematic southward bias in the EBM-predicted cross-equator transport. This is likely because the EBM does not capture the fact that the NH warms up more than the SH even in the absence of cross-equatorial energy source differences. As shown in Figure 7(d), there is a systematic tendency towards more clear-sky OLR increase in the NH compared with the SH. The EBM cannot capture this effect, and hence has a southward bias in the cross-equatorial energy transport, In addition to the bias from the temperature effect, the

EBM treats the water vapor effect as a function of surface temperature alone, and thus only captures the enhanced greenhouse warming that results from increasing saturation vapor pressure. The EBM therefore also underestimates the changes in water vapor associated with the ITCZ shift, leading to an error that is positively correlated with the shift. Models that have more southward ITCZ shift (red models) tend to have the largest southward energy transport bias, because they are missing the heating in the SH from increasing water vapor content.

Having shown that the energetic framework does a good job at separating the model-to-model differences in ITCZ shifts, we run single forcing experiments with the EBM to attribute the ITCZ shifts to individual energy source terms. The result is plotted in Figure 10. Clouds (plotted as the sum of SW and LW effects, due to the cancellation of these effects in the tropics) still contribute the large majority of the spread. In the multimodel mean, clouds cause no systematic effect, but they contribute a very large fraction of the model-to-model differences. The other terms are non-negligible though: predictions with cloud energetic terms alone are worse than the relation given in Figure 9 (not shown). The effects of surface albedo (I) and surface flux (O) are smaller than in Figure 8 due to the fact that these terms are located primarily in higher latitudes, and less of their effect is felt at the equator in the diffusive model (more of the energy source is offset by OLR change on the way to the tropics). Both surface albedo and surface flux are still significant. Changes in surface albedo cause a systematic southward cross-equatorial energy transport and northward ITCZ shift in nearly all models, due to more ice melting in the NH mid-latitudes, where it can be communicated more easily to the equator as compared with the high latitude sources in the SH. Surface flux changes cause a small northward cross-equatorial transport in some models, and a small southward transport in others. The non-cloud shortwave term (N_S) causes a small southward energy transport in nearly all models.

As a classification of the importance of different latitude bands in the EBM, we plot the EBM prediction using only tropical energy sources (setting the energy sources to be zero poleward of 20N/20S), and the prediction using only extratropical energy sources in Figure 11. It is clear that considering tropical forcings alone is insufficient to explain the model-to-model spread in changes in cross-equator transport. On the other hand, by prescribing extratropical energy sources only, the EBM is able to capture most of the spread. The correlation coefficient between the predicted change in transport and the actual change in transport in GCMs is 0.86, compared with a correlation coefficient of 0.36 for tropical forcings alone. We thus argue that the ITCZ response in the model is largely driven by the extratropics, with the tropics providing a positive feedback on the shifts via the water vapor and cloud LW effects.

5. Conclusions

The most uncertain region for projections of precipitation with global warming is the tropics (IPCC 2007). In slab ocean simulations, we have shown that this is largely due to variations in the direction of the shift of the ITCZ, and precipitation changes are felt in an approximately zonally symmetric manner across the tropics. We also have demonstrated a clear relationship between cross-equatorial atmospheric energy transport change and the direction of the ITCZ shift in these models, implying that one can explain the shift in the ITCZ by explaining the cross-equatorial energy transport. Southward shifts of the ITCZ occur due to more positive energy sources into the SH atmosphere than the NH, which cause northward anomalous energy transports across the equator, and a concurrent southward shift of ITCZ.

Any change in the atmospheric energy budget has the potential to influence the cross-

equatorial energy transport. We investigate the hemispheric asymmetry of each energy source, and quantify its influence on the cross-equatorial energy transport with two methods: (1) integrating the change in the atmospheric energy budget after removing the global mean of each source to calculate the implied change in cross-equatorial transport, and (2) prescribing the energy source term in an EBM and analyzing the amount of cross-equatorial transport change assuming diffusive transport. The first method provides an exact partitioning, where the contributions of the individual terms add up to the total change in cross-equatorial transport. The second method takes into account the local change in non-cloud OLR caused by each energy source term. A heating of the atmosphere is balanced to a large extent by increasing OLR due to local warming. Especially for energy sources far from the equator, only a small fraction of a given heating will translate into a cross-equatorial energy transport. The EBM attribution method provides a method to calculate the partition between energy transported across the equator and changes in OLR, and thus gives a better depiction of how tropical precipitation would shift if this term was removed. The EBM does not, on the other hand, simulate the changes in water vapor content associated with shifts in tropical precipitation, which provide a positive feedback to any shift (Yoshimori and Broccoli 2009).

With both attribution methods, we conclude that clouds cause most of the discrepancies among models. Changes in surface fluxes (which exist despite the fact that these are slab equilibrium simulations) and surface albedo each contribute a non-negligible amount to cross-equatorial transport changes and ITCZ shifts. Using the EBM, we also quantify the effect of tropical and extratropical energy source terms on the shifts. Tropical water vapor changes provide a positive feedback to any shift in the ITCZ, through drying and enhanced radiative cooling of the hemisphere that the ITCZ shifts away from, and moistening and enhanced greenhouse warming of the hemisphere which the ITCZ shifts towards. By considering the

changes in the atmospheric energy budget due to clouds, ice, and surface fluxes in the extratropics only, however, we can explain most of the spread in cross-equatorial transport among GCMs. This implies that most of the discrepancies in the ITCZ shifts are due to differences in energetic responses in the extratropics. This result underscores the importance of simulating climate responses from clouds, sea ice, snow, and water vapor with fidelity. In addition to their importance for local climate, they can have a strong nonlocal impact on tropical precipitation by creating northward or southward shifts in the ITCZ. Ocean heat transport changes can have similar effects on shifting the ITCZ, and we will quantify the importance of this term in future studies of coupled GCM simulations of global warming.

6. Acknowledgements

We acknowledge helpful conversations with John Chiang, Sarah Kang, Dennis Hartmann, and Mark Zelinka. DMWF is supported by NSF Grants ATM-0846641 and AGS-0936069, and a University of Washington Royalty Research Fund grant.

REFERENCES

Broccoli, A. J., K. A. Dahl, and R. J. Stouffer, 2006: Response of the ITCZ to Northern Hemisphere cooling. *Geophys. Res. Lett.*, **33**, L01 702, doi:10.1029/2005GL024 546.

Cheng, W., C. M. Bitz, and J. C. H. Chiang, 2010: Adjustment of the global climate to an abrupt slowdown of the atlantic meridional overturning circulation. *Ocean Circulation: Mechanisms and Impacts*, S. Chiang and Hemming, Eds., AGU Monographs, in press.

Chiang, J. C. H., M. Biasutti, and D. S. Battisti, 2003: Sensitivity of the Atlantic ITCZ to Last Glacial Maximum boundary conditions. *Paleoceanography*, **18**, doi:10.1029/2003PA000 916.

Chiang, J. C. H. and C. M. Bitz, 2005: Influence of high latitude ice cover on the marine Intertropical Convergence Zone. *Climate Dyn.*, **25**, 477–496.

Chiang, J. C. H., W. Cheng, and C. M. Bitz, 2008: Fast teleconnections to the tropical Atlantic sector from Atlantic thermohaline adjustment. *Geophys. Res. Lett.*, **35**, L07 704, doi:10.1029/2008GL033 292.

Donohoe, A. and D. S. Battisti, 2011: What determines meridional heat transport in climate models? *Submitted to J. Climate*.

Held, I. M. and B. J. Soden, 2006: Robust responses of the hydrological cycle to global warming. *J. Climate*, **19**, 5686–5699.

Horel, J. D. and J. M. Wallace, 1981: Planetary-scale atmospheric phenomena associated with the Southern Oscillation. *Mon. Wea. Rev.*, **109**, 813–829.

Hoskins, B. J. and D. J. Karoly, 1981: The steady linear response of a spherical atmosphere to thermal and orographic forcing. *J. Atmos. Sci.*, **38**, 1179–1196.

Hwang, Y.-T. and D. M. W. Frierson, 2010: Increasing atmospheric poleward energy transport with global warming. *Geophys. Res. Lett.*, **37 (24)**, L24 807, doi:10.1029/2010GL045 440.

Hwang, Y.-T., D. M. W. Frierson, I. M. Held, and B. J. Soden, 2011: Corrigendum to Held and Soden (2006). *J. Climate*, **24 (5)**, 1559–1560.

Kang, S. M., D. M. W. Frierson, and I. M. Held, 2009: The tropical response to extratropical thermal forcing in an idealized GCM: The importance of radiative feedbacks and convective parameterization. *J. Atmos. Sci.*, **66**, 2812–2827, doi:10.1175/2009JAS2924.1.

Kang, S. M., I. M. Held, D. M. W. Frierson, and M. Zhao, 2008: The response of the ITCZ to extratropical thermal forcing: idealized slab-ocean experiments with a GCM. *J. Climate*, **21**, 3521–3532.

Koutavas, A. and J. Lynch-Stieglitz, 2004: Variability of the marine ITCZ over the eastern Pacific during the past 30,000 years: Regional perspective and global context. *The Hadley Circulation: Present, Past, and Future*, H. F. Diaz and R. S. Bradley, Eds., Springer, 347–369.

Lea, D. W., D. K. Pak, L. C. Peterson, and K. A. Hughen, 2003: Synchronicity of tropical and high-latitude Atlantic temperatures over the last glacial maximum. *Science*, **301**, 1361–1364.

Lin, J.-L., 2007: The double-ITCZ problem in IPCC AR4 coupled GCMs: Ocean-atmosphere feedback analysis. *J. Climate*, **20**, 4497–4525.

Pahnke, K., J. P. Sachs, L. Keigwin, A. Timmerman, and S. P. Xie, 2007: Eastern tropical Pacific hydrologic changes during the past 27,000 years from D/H ratios in alkenones. *Paleoceanography*, **22**, PA4214, doi:10.1029/2007PA001 468.

Sachs, J. P., D. Sachse, R. H. Smittenberg, Z. Zhang, D. S. Battisti, and S. Golubic, 2009: Southward movement of the Pacific intertropical convergence zone AD 1400-1850. *Nature Geoscience*, **2**, 519–525, doi:10.1038/NGEO554.

Soden, B. J., I. M. Held, R. Colman, K. M. Shell, J. T. Kiehl, and C. A. Shields, 2008: Quantifying climate feedbacks using radiative kernels. *J. Climate*, **21**, 3504–3520.

Taylor, K. E., M. Crucifix, P. Braconnot, C. D. Hewitt, C. Doutriaux, A. J. Broccoli, J. F. B. Mitchell, and M. J. Webb, 2007: Estimating shortwave radiative forcing and response in climate models. *J. Climate*, **20**, 2530–2543.

Trenberth, K. E. and D. P. Stepaniak, 2003: Covariability of components of poleward atmospheric energy transports on seasonal and interannual timescales. *J. Climate*, **16**, 3691–3705.

Wu, Y., M. Ting, R. Seager, H.-P. Huang, and M. A. Cane, 2010: Changes in storm tracks and energy transports in a warmer climate simulated by the GFDL CM2.1 model. *Climate Dyn.*, **37**, 53–72.

Yoshimori, M. and A. J. Broccoli, 2008: Equilibrium response of an atmosphere-mixed layer ocean model to different radiative forcing agents: global and zonal mean response. *J. Climate*, **21**, 4399–4423, doi:10.1175/2008JCLI2172.1.

Yoshimori, M. and A. J. Broccoli, 2009: On the link between Hadley circulation changes and radiative feedback processes. *Geophys. Res. Lett.*, **36**, L20 703, doi:10.1029/2009GL040 488.

Zelinka, M. D. and D. L. Hartmann, 2011: Climate feedbacks, and their implications for poleward energy flux changes in a warming climate. *in revision, J. Climate*.

Zhang, R. and T. L. Delworth, 2005: Simulated tropical response to a substantial weakening of the Atlantic thermohaline circulation. *J. Climate*, **18**, 1853–1860.

List of Figures

6 Energy source terms into the atmosphere (W/m^2) due to (a) the surface albedo effect, (b) the change in upward surface flux, (c) the non-cloud SW effect, and (d) the LW residual term of the kernel method. (e)-(h) The antisymmetric component of the energy source term, $\frac{1}{2}(Q(-\phi)-Q(\phi))$, where Q is the change of the atmospheric energy budget due to the terms in (a)-(d), respectively. The models are colored as in Figure 1. 35

7 Energy source terms into the atmosphere (W/m^2) due to (a) the temperature effect, (b) the sum of the water vapor and temperature effects, and (c) the total change in atmospheric energy budget minus the water vapor and temperature effects. (d)-(f) The antisymmetric component of the energy source term, $\frac{1}{2}(Q(-\phi)-Q(\phi))$, where Q is the change of the atmospheric energy budget associated with the terms in (a)-(c), respectively. The models are colored as in Figure 1. 36

8 Attribution of the cross-equatorial energy flux (PW) analyzed by the exact integration method to atmospheric energy sources from the LW cloud effect (C_L), the SW cloud effect (C_S), the total cloud effect ($C_L + C_S$), the water vapor plus temperature LW effect ($WV + T$), the surface albedo effect (I), the change in upward surface flux (O), the LW residual term (R_L), and the non-cloud SW effect (N_S). The models are colored as in Figure 1. The X symbol denotes the multi-model mean in each column. 37

9 The EBM-predicted change in cross-equator flux ($F_P(\phi = 0)$) in PW versus the actual change in cross-equator flux ($F_A(\phi = 0)$). The models are colored as in Figure 1. 38

11 (a) The EBM-predicted change in cross-equator flux ($F_P(\phi = 0)$) in PW using only tropical energy sources versus the actual change in cross-equator flux ($F_A(\phi = 0)$). (b) The EBM-predicted change in cross-equator flux ($F_P(\phi = 0)$ in PW using only extratropical energy sources versus the actual change in cross-equator flux ($F_A(\phi = 0)$). The models are colored as in Figure 1. 40

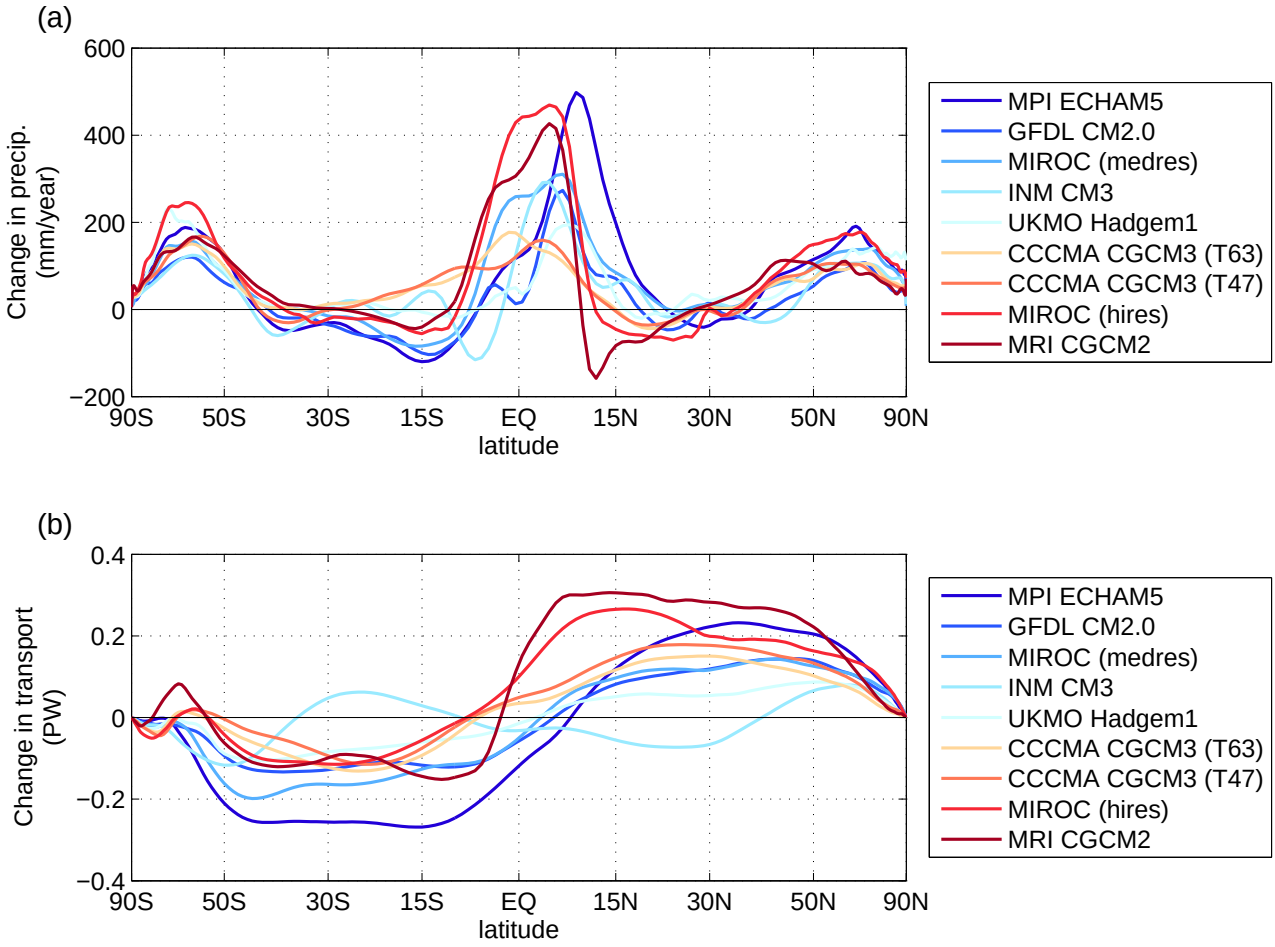

FIG. 1. (a) The zonally averaged precipitation change (mm/yr) between the slab ocean control experiment and the $2 \times CO_2$ equilibrium experiment. (b) The change in northward energy transport in the atmosphere (PW). In both subplots, the models are colored according to their cross-equatorial energy transport in panel (b), with blue representing a more southward transport and red representing a more northward transport.

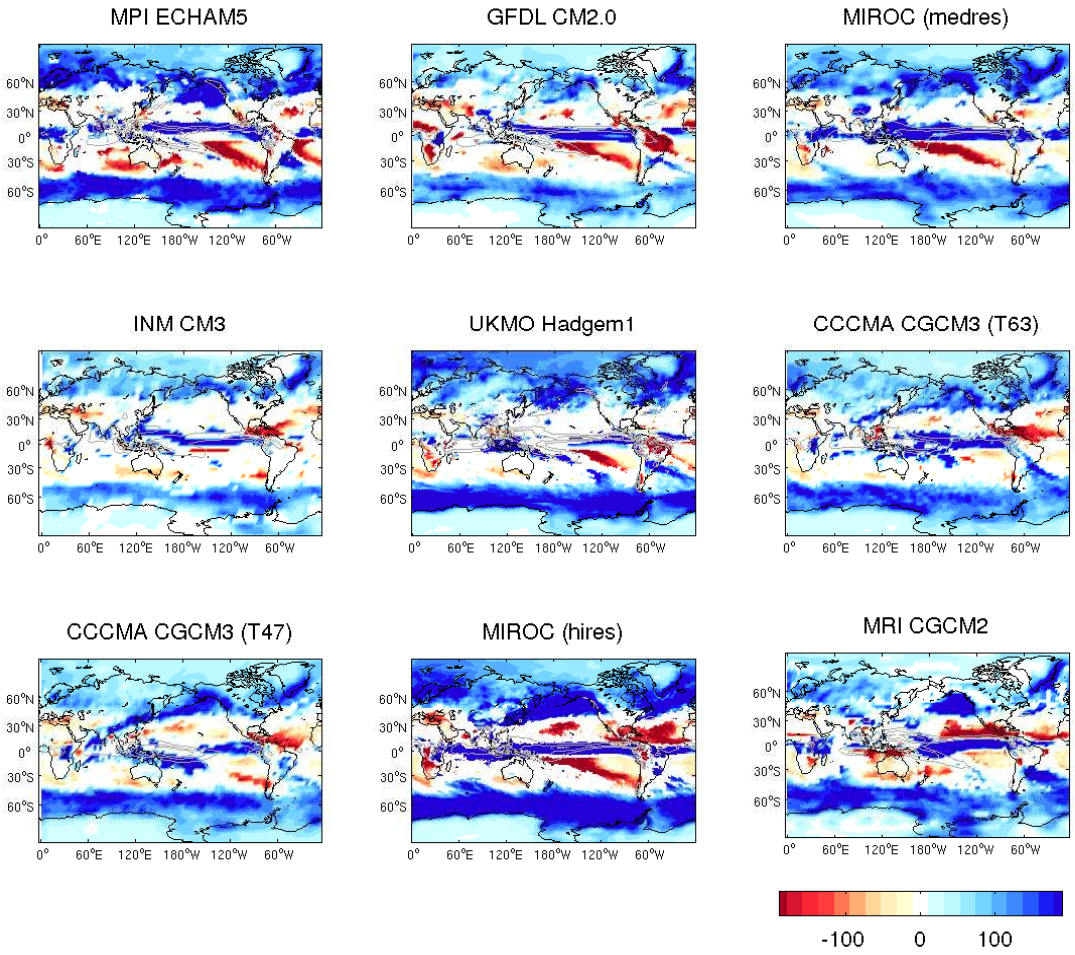

FIG. 2. The precipitation change (mm/yr, colors) and precipitation in the control experiment (contours, 1000, 1500, 2500, and $4000mm/yr$).

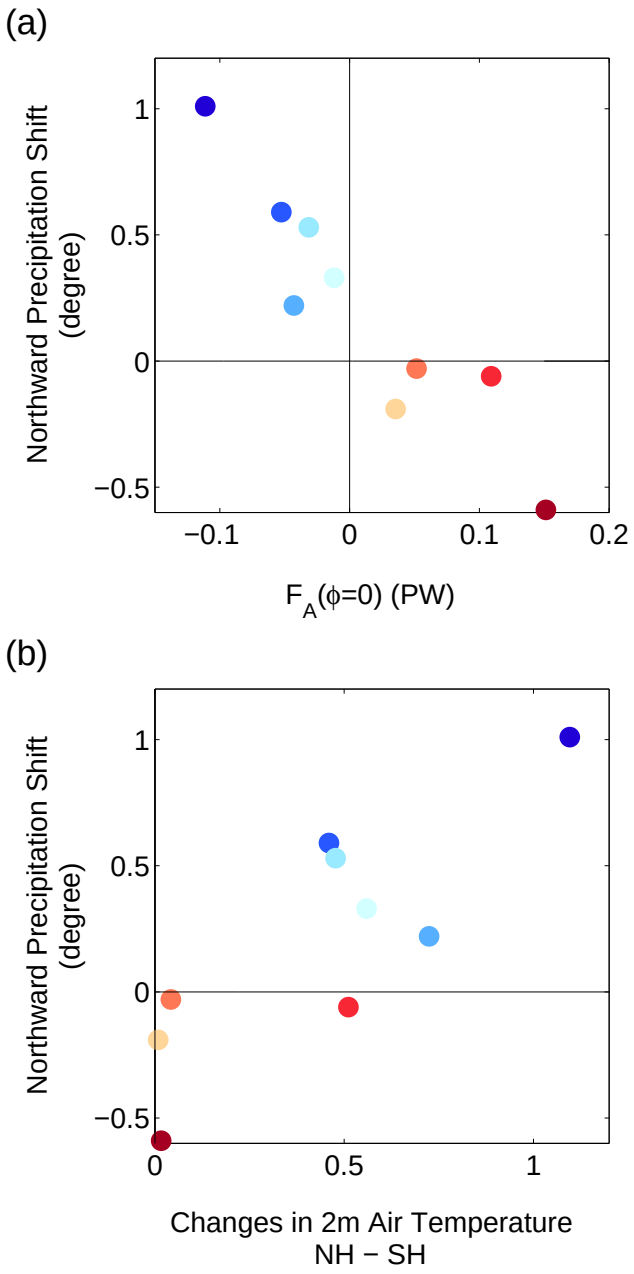

FIG. 3. (a) The shift of the precipitation center (degrees, see text for definition) versus the change in atmospheric energy transport at the equator ($F_A(\phi = 0)$). (b) The shift in precipitation center (degrees) versus the 2 meter air temperature change averaged in the NH minus SH. The models are colored as in Figure 1.

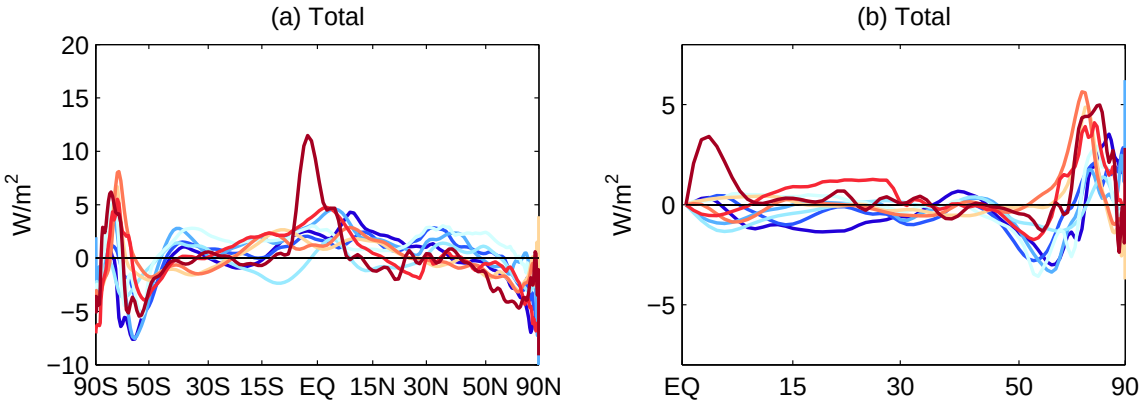

FIG. 4. (a) The total change of the atmospheric energy budget (Q_A) in W/m^2. (b) The antisymmetric component of the change of the atmospheric energy budget ($\frac{1}{2}(Q_A(-\phi) - Q_A(\phi))$ in W/m^2. The models are colored as in Figure 1.

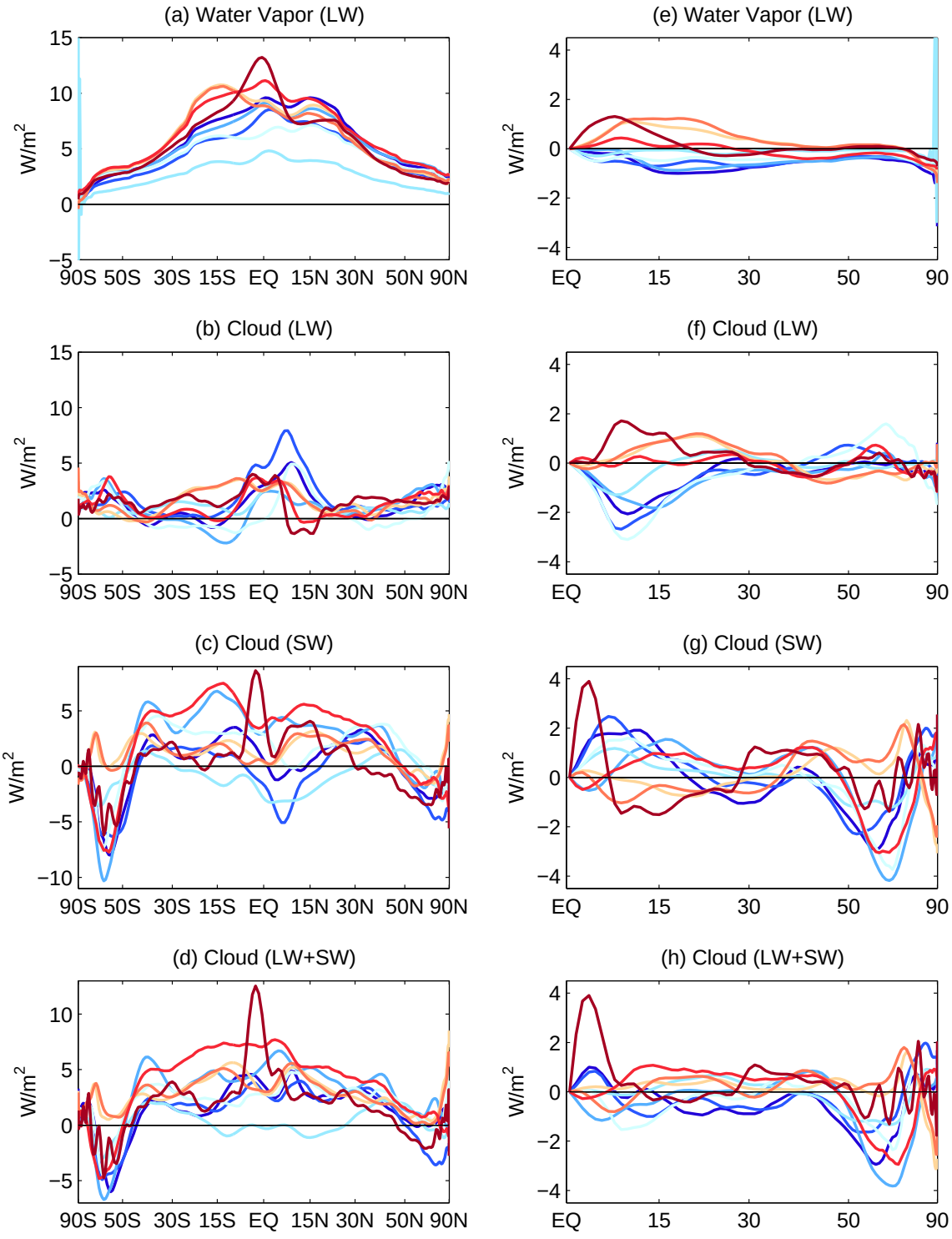

FIG. 5. Energy source terms into the atmosphere (W/m^2) due to (a) the water vapor LW effect, (b) the cloud LW effect, (c) the cloud SW effect, and (d) the total cloud (LW+SW) effect. (e)-(h) The antisymmetric component of the energy source term, $\frac{1}{2}(Q(-\phi) - Q(\phi))$, where Q is the change in atmospheric energy budget due to the terms in (a)-(d), respectively. The models are colored as in Figure 1.

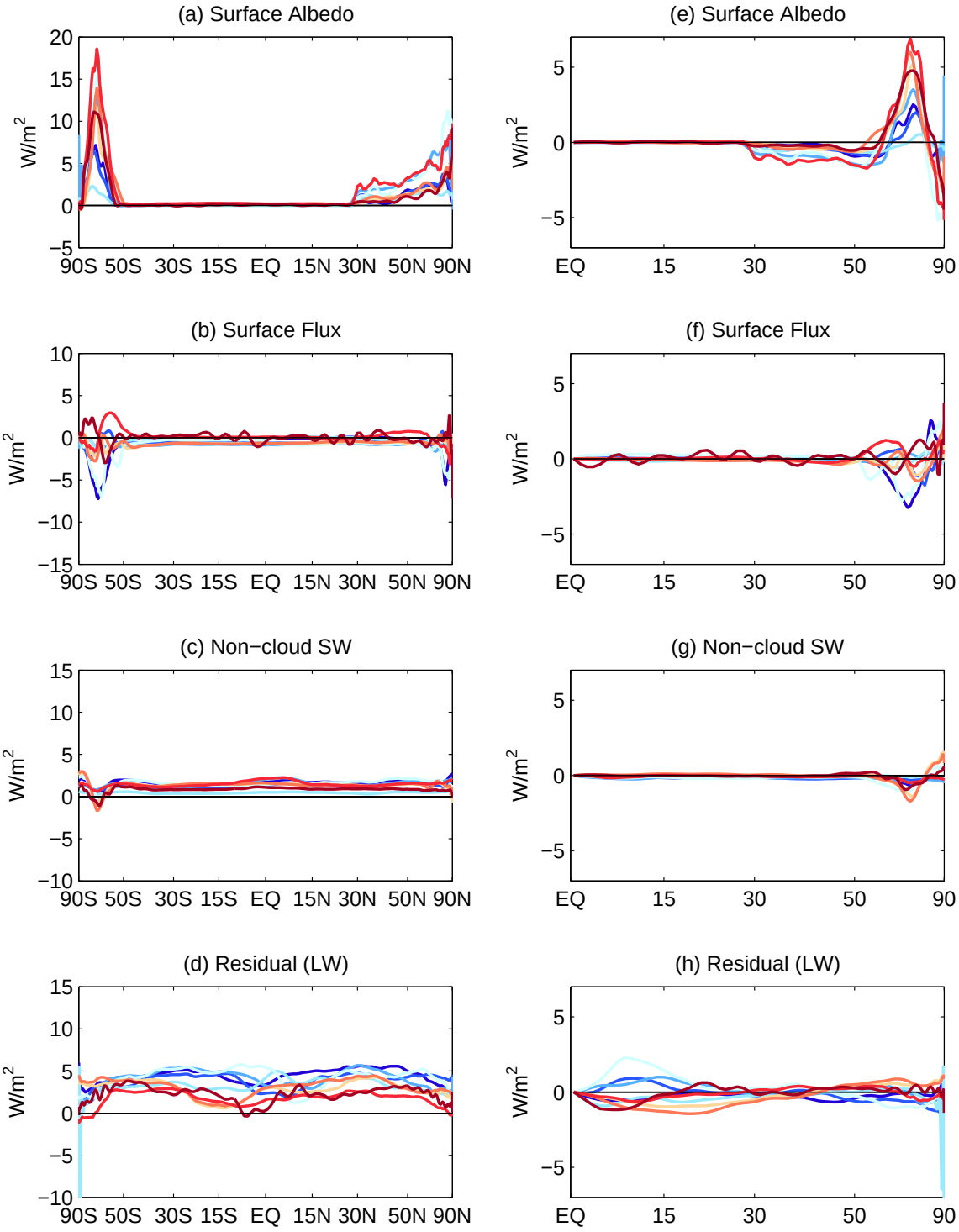

FIG. 6. Energy source terms into the atmosphere (W/m^2) due to (a) the surface albedo effect, (b) the change in upward surface flux, (c) the non-cloud SW effect, and (d) the LW residual term of the kernel method. (e)-(h) The antisymmetric component of the energy source term, $\frac{1}{2}(Q(-\phi) - Q(\phi))$, where Q is the change of the atmospheric energy budget due to the terms in (a)-(d), respectively. The models are colored as in Figure 1.

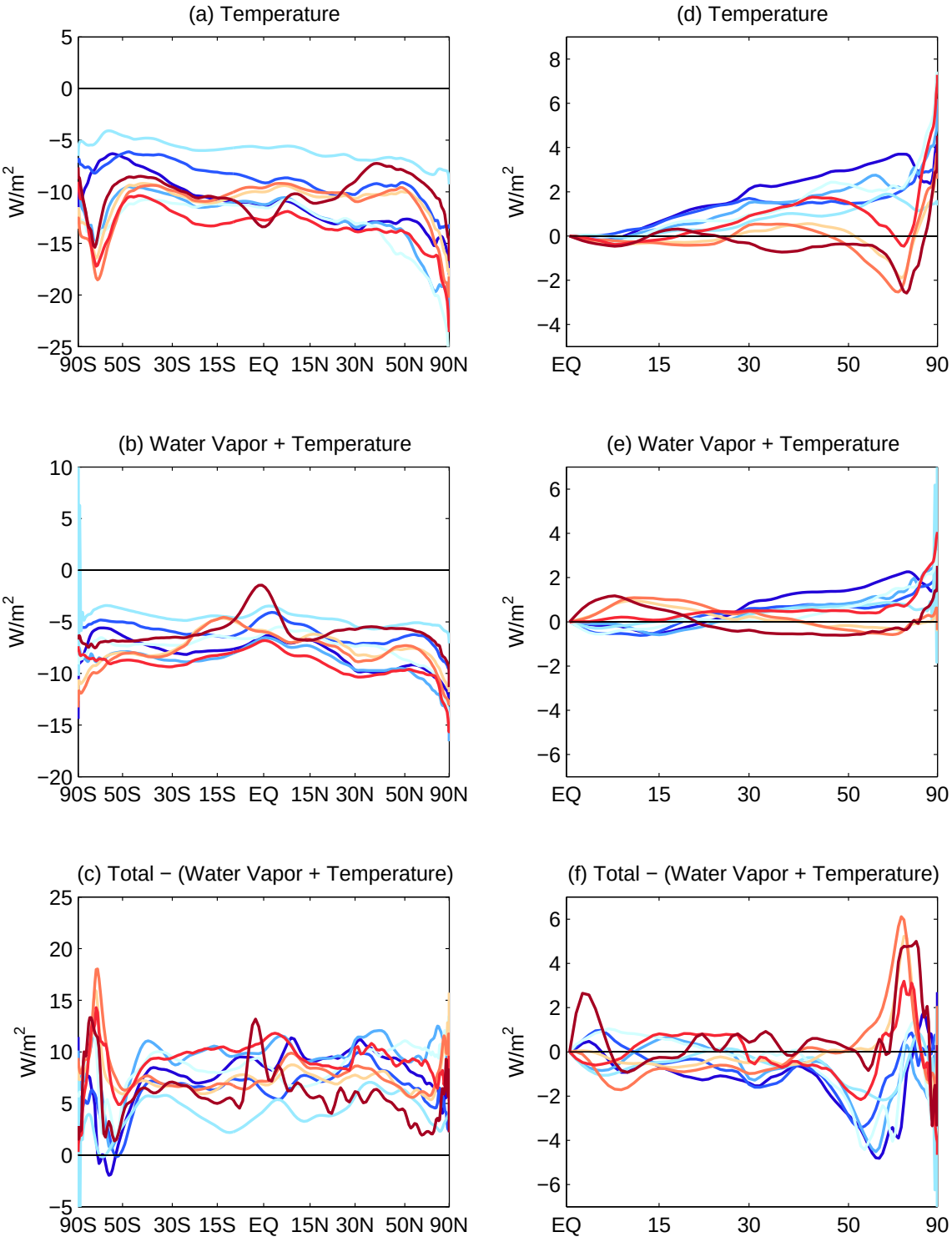

FIG. 7. Energy source terms into the atmosphere (W/m^2) due to (a) the temperature effect, (b) the sum of the water vapor and temperature effects, and (c) the total change in atmospheric energy budget minus the water vapor and temperature effects. (d)-(f) The antisymmetric component of the energy source term, $\frac{1}{2}(Q(-\phi) - Q(\phi))$, where Q is the change of the atmospheric energy budget associated with the terms in (a)-(c), respectively. The models are colored as in Figure 1.

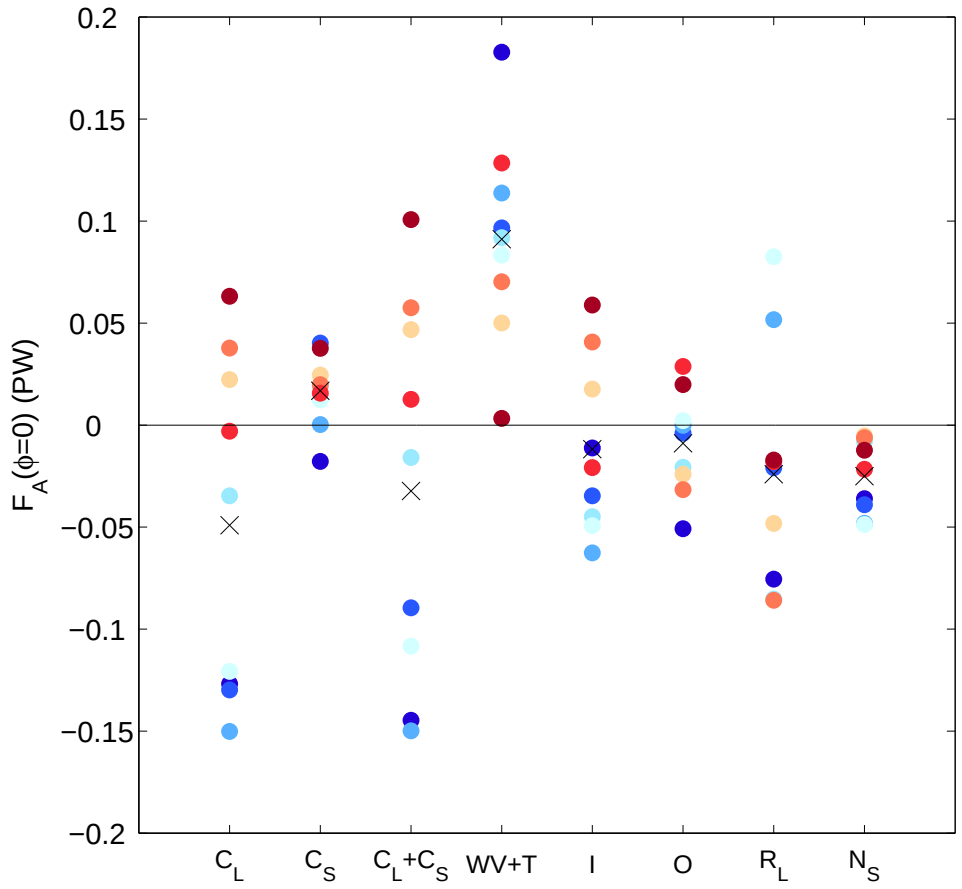

FIG. 8. Attribution of the cross-equatorial energy flux (PW) analyzed by the exact integration method to atmospheric energy sources from the LW cloud effect (C_L), the SW cloud effect (C_S), the total cloud effect ($C_L + C_S$), the water vapor plus temperature LW effect ($WV + T$), the surface albedo effect (I), the change in upward surface flux (O), the LW residual term (R_L), and the non-cloud SW effect (N_S). The models are colored as in Figure 1. The X symbol denotes the multi-model mean in each column.

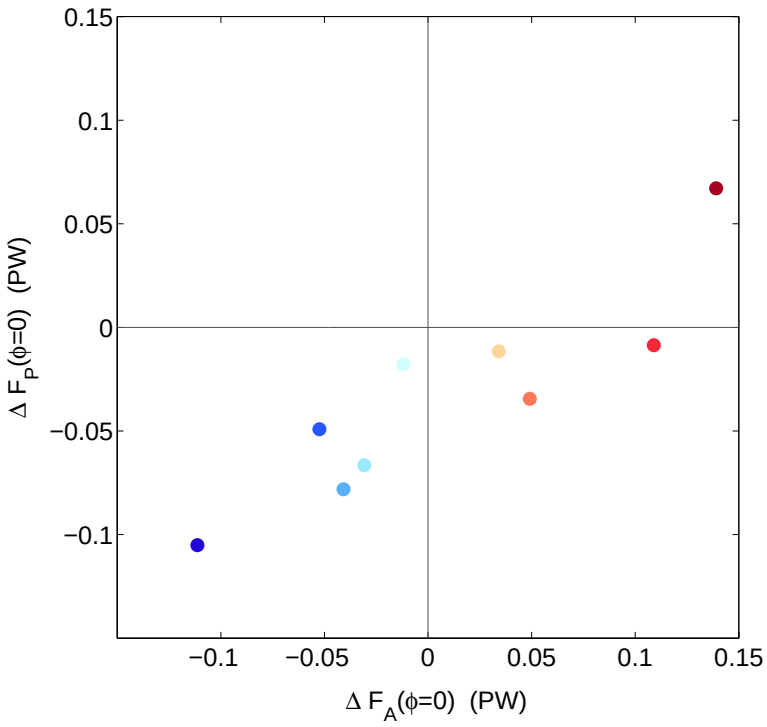

FIG. 9. The EBM-predicted change in cross-equator flux ($F_P(\phi = 0)$) in PW versus the actual change in cross-equator flux ($F_A(\phi = 0)$). The models are colored as in Figure 1.

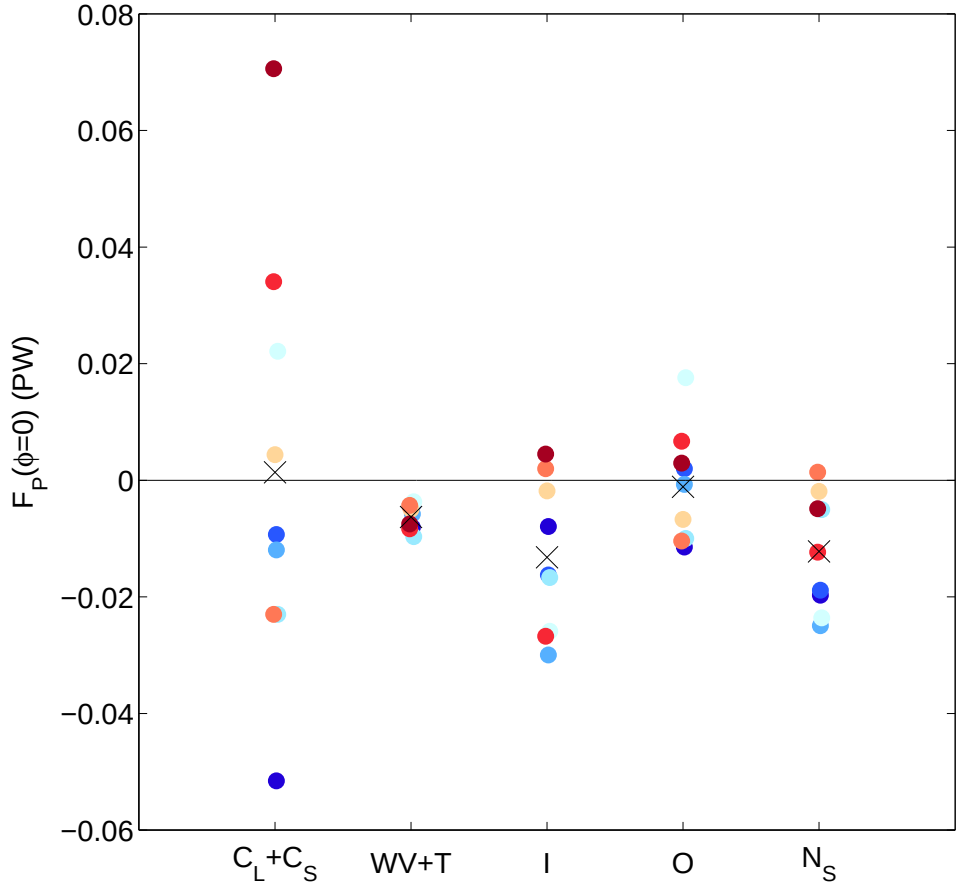

FIG. 10. Attribution of the cross-equatorial energy flux (PW) calculated from the EBM method to atmospheric energy sources from the total cloud effect ($C_L + C_S$), the water vapor plus temperature LW effect ($WV + T$), the surface albedo effect (I), the change in upward surface flux (O), and the non-cloud SW effect (N_S). The models are colored as in Figure 1. The X symbol denotes the multi-model mean in each column.

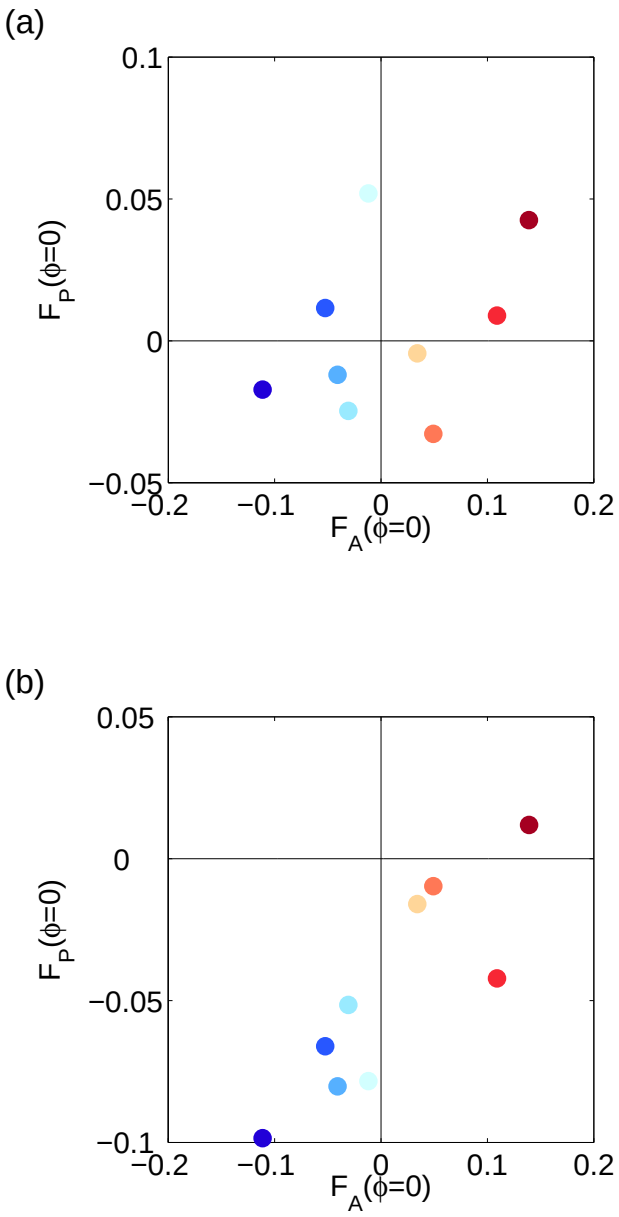

FIG. 11. (a) The EBM-predicted change in cross-equator flux ($F_P(\phi = 0)$) in PW using only tropical energy sources versus the actual change in cross-equator flux ($F_A(\phi = 0)$). (b) The EBM-predicted change in cross-equator flux ($F_P(\phi = 0)$ in PW using only extratropical energy sources versus the actual change in cross-equator flux ($F_A(\phi = 0)$). The models are colored as in Figure 1.